RESEARCH PAPER

Study of Lightning-Induced Disturbances in Distribution Systems

Dr Shraddha Sharma*[1] Dr Archana Pouranik[2] , Dr Rajeshwari Gour[3]

[1*]Associate Professor of Physics , Oriental Institute of Science and Technology, Bhopal - 462022, Madhya Pradesh, India , Email: shraddhasharma@oriental.ac.in, Orcid id - https://orcid.org/0009-0006-4227-0668
[2]Associate Professor of Chemistry , Oriental Institute of Science and Technology, Bhopal - 462022, Madhya Pradesh, India , Email: archanapouranik@oriental.ac.in, Orcid id -0009-0006-5787-961X
[3]Assistant Professor of Chemistry , Oriental Institute of Science and Technology Bhopal - 462022, Madhya Pradesh, India , Email: rajeshwarigaur@oriental.ac.in

Abstract
Overvoltage caused by lightning is also a serious risk to the insulation of distribution feeders, terminals of transformers, and other equipment under protection. This paper suggests a combined MATLAB/Simulink-based model of assessing the direct and indirect lightning surge propagation in a three-phase distribution feeder with coordinated protection elements. The model is a combination of a double-exponential source of lightning, a three-phase coupling of matrices, an RLC feeder response, a nonlinear metal-oxide varistor (MOV) arrester behavior, a grounding impedance, and flashover detection. The simulation of direct surge cases with 20 kV to 1 MV, indirect lightning current-coupling cases, variations in grounding resistance and flashover threshold sensitivities were simulated to evaluate system-level and component-level performance. The results indicate that the MOV arrester dropped the unprotected voltage in the case of the peak current of 40 kA, to 35.47 kV and then to 22.34 kV under the baseline surge case. Final equipment stress was strongly influenced by grounding resistance; with Rg increasing to 10 Ω, the final equipment voltage rose by a factor of 2.5. The integrated direct surge analysis indicated flashover at the 1 MV case, although there was MOV clamping, due to the rise in grounding voltages. The advanced model decreased final equipment voltage by an average of 95.77% to 99.69% across integrated scenarios compared to the basic unprotected feeder model. The paper shows that effective lightning protection evaluation should take into account the feeder coupling, transformer transfer, arrester stress, grounding response, and insulation margin all at the same time.

Keywords: Lightning-induced overvoltage; MOV surge arrester; distribution feeder protection; grounding voltage rise; flashover detection.
How to cite this article: Sharma S, Pouranik A, Gour R. Study of Lightning-Induced Disturbances in Distribution Systems. Int J Drug Deliv Technol. 2026;16(55s): 677-697. DOI: 10.25258/ijddt.16.55s.69

Nomenclature

Symbol / Term	Description	Unit
$v_L(t)$	Direct lightning surge voltage	V
V_p	Peak value of applied direct surge voltage	V or kV
α, β	Double-exponential voltage waveform shaping coefficients	s^{-1}
$i_L(t)$	Lightning current waveform	A
I_p	Peak lightning current	A or kA
α_i, β_i	Double-exponential current waveform shaping coefficients	s^{-1}
$v_{\text{ind}}(t)$	Indirect lightning-induced feeder voltage	V
M	Electromagnetic coupling coefficient	H or μH
$H_f(s)$	RLC feeder transfer function	—
$H_T(s)$	Transformer surge transfer function	—
R	Feeder resistance	Ω
L	Feeder inductance	H
C	Feeder capacitance	F
K_{phase}	Matrix-based three-phase coupling coefficient matrix	—
$v_A(t)$, $v_B(t)$, $v_C(t)$	Coupled phase voltages of phases A, B, and C	V
$V_A(s)$, $V_B(s)$, $V_C(s)$	Laplace-domain phase voltages	V
k_T	Transformer voltage ratio	—
$V_p(s)$	Transformer primary-side voltage in Laplace domain	V
$V_s(s)$	Transformer secondary-side voltage in Laplace domain	V
K_c	Enhanced transformer coupling coefficient	—
$V_{sat,core}$	Transformer core saturation reference voltage	V
I_{MOV}	MOV arrester current	A
V_{MOV}	MOV arrester voltage	V
f_{MOV}	Manufacturer-based MOV nonlinear voltage-current characteristic	—

*Author for Correspondence: shraddhasharma@oriental.ac.in

I_{max}	Maximum MOV current limit	A or kA
$V_{protected}(t)$	MOV-protected voltage	V
$P_{MOV}(t)$	Instantaneous MOV power indicator	W
E_{MOV}	Approximate MOV energy indicator	J
R_g	Grounding resistance	Ω
L_g	Grounding inductance	H
$i_g(t)$	Grounding current	A
$v_g(t)$	Ground voltage rise	V
$v_{eq}(t)$	Final equipment voltage	V
$V_{flashover}$	Flashover threshold / insulation withstand voltage	V or kV
$M_{ins}(t)$	Instantaneous insulation margin	V
M_{min}	Minimum insulation margin	V or kV
F(t)	Instantaneous flashover indicator	0 or 1
F_{case}	Case-level flashover status	0 or 1
V_{peak}	Peak value of a voltage waveform	V or kV
$I_{MOV,peak}$	Peak MOV current	A
$V_{g,peak}$	Peak ground voltage rise	V or kV
$V_{eq,peak}$	Peak final equipment voltage	V or kV
η	Voltage reduction percentage	%
η_{adv}	Advanced model reduction relative to basic feeder model	%
T_{sim}	Total simulation time	s
MOV	Metal-oxide varistor surge arrester	—
RLC	Resistance–inductance–capacitance feeder model	—

1. Introduction

Overvoltage caused by lightning is still considered one of the most significant sources of transient stress, insulation degradation and malfunctioning of protection devices in overhead and distribution power networks. The natural lightning activity can cause large induced voltages on distribution feeders, and field measurements have shown that these overvoltages are highly dependent on the characteristics of lightning, the line configuration, and the coupling conditions [1]. Other related concerns have been reported on the similar transient overvoltage concerns, in the renewable-energy-connected systems, where lightning strikes have been known to cause severe voltage stress across electrical components and connected equipment [2]. In the case of medium-voltage distribution networks, induced overvoltage distribution is of particular concern since nearby lightning can have an indirect effect on the line, but still can induce high transient voltages in the distribution network through electromagnetic coupling [3]. Transient effects due to lightning on cable and photovoltaic systems are further confirmed by numerical studies of transient effects on cable and photovoltaic systems [4]. In spite of this, there is still a need to have an integrated modeling approach that would link the surge source, feeder response, transformer transfer, surge arrester operation, grounding effect, and insulation withstand capability. Microgrids and low-voltage AC distribution systems can be affected by lightning impulses that can introduce short-duration yet high-amplitude disturbances that can exceed component withstand levels [5]. Furthermore, the various terminal loads, grounding dissipation paths, and the secondary cables and equipment connected to a substation are also influenced by different terminal loads and grounding dissipation paths, which makes grounding and equipment-side voltage rise significant components of transient evaluation [6]. It may thus be insufficient to have a model that merely estimates the overvoltage on the feeder side in order to determine the actual stress on the equipment being protected. The issue that is the focus of the present research is the lack of complete protection-chain behavior in simple simulations of feeder surges. The simplified model of RLC feeder can be used to estimate the nonlinear response to overvoltage without protection, but cannot model the phase-to-phase coupling, transformer surge transfer, nonlinear MOV arrester clamping, grounding voltage rise, or flashover risk. More recent efforts to assess lightning outage and surrogate model also reveal the necessity to have efficient but physically meaningful models to analyze lightning-related failures in power systems [7]. In the same way, research on lightning effects in photovoltaic systems demonstrates that highly detailed simulation models can be used to assess complex surge propagation paths, and equipment-level stress [8].

This paper comes up with a combination of MATLAB/Simulink-based lightning protection model of a three-phase distribution feeder. The model involves direct surge excitation, indirect lightning induced voltage coupling, matrix based three phase feeder coupling, transformer surge transfer, nonlinear MOV surge arrester behavior, grounding impedance and flashover detection. The study is restricted to simulation-based transient analysis and the model consists of simplified equivalent representations instead of the full electromagnetic field or the network modeling with a geographical detail. However, the method suggested is important since it considers the end equipment voltage and insulation margin instead of just the magnitude of the surge at the feeder-side. This is significant to practical protection assessment since lightning protection and system-level risk assessment studies indicate that effective mitigation requires not only

understanding of the surge behavior but also a system-level risk assessment [9]. Moreover, the direct lightning effects on grounding networks can generate large secondary transients, which further justifies the importance of considering grounding and equipment-side voltage raise in the model [10].

The primary aim of the study is to develop and model an integrated lightning protection system to compare the unprotected feeder response with the response of the advanced protective equipment. The specific objectives are:

- To simulate direct lightning surge excitation, as well as indirect lightning-induced voltage coupling in a three-phase distribution feeder.
- To test the phase coupling of matrices and transfer of transformer surge to transient conditions caused by lightning.
- To examine the nonlinear MOV surge arrester performance in the form of voltage clamping, arrester current, and energy stress.
- To measure how grounding impedance, and flashover threshold affect the ultimate equipment voltage and insulation safety.
- To make a comparison between the basic unprotected feeder model and the advanced integrated protection model with the use of the voltage reduction, final equipment stress, and flashover status.

2. Literature Review

Recent research on transients caused by lightning has more and more highlighted the importance of considering the propagation of surges beyond the original point of disturbance. Zhou et al. [11] characterized the transient voltage characteristics in buried power cables due to lightning-induced transients and the effects of the soil dissipation effects on transient voltage. They find that the medium and grounding environment surrounding the object of lightning strike can greatly influence the intensity and spreading of the voltages caused by lightning strike. The result is applicable to distribution feeder protection since grounding impedance and earth-return paths may cause the final voltage stress to be experienced by equipment.

The use of computational techniques to estimate voltages caused by lightning on overhead distribution lines has also been widely used. A computation of the induced voltages using RBF-FDTD-based approach was proposed by Vu et al. [12] who demonstrated that numerical field and circuit techniques are helpful in assessing lightning impact on distribution networks. Their work justifies the application of a simulation-based modeling to estimate the overvoltage behavior under various lightning and feeder conditions. Complete electromagnetic treatments may however be computationally expensive, particularly when it is necessary to repeat parametric studies.

Detection and identification of lightning-related phenomena in power systems are some of the other areas that other researchers have focused on. Zhong et al. [13] came up with a lightning strike identification algorithm of an all-parallel auto-transformer traction power supply system based on morphological fractal theory. Their work shows that it is possible to differentiate between lightning transients and other disturbances with the help of signal-processing-based techniques. In a similar fashion, Wang et al. [14] introduced a severity estimation technique of the voltage sags caused by lightning using multi platform monitoring data. These studies demonstrate that lightning events need to be accurately modeled and have effective performance indicators to assess severity and operational risk.

The modeling of surge arrester has also been considered in the analysis of the distribution system. In a power distribution system, Ibrahim et al. [15] investigated the simulation of lightning and surge arrester in a power distribution system, and the importance of the placement of arrester and the surge limiting behavior. Their contribution is directly connected with the current research since MOV surge arresters are at the core of restricting overvoltage. Nevertheless, the clamped voltage is not the only criterion to evaluate arrester performance; arrester current, energy stress, and grounding voltage rise should also be taken into account.

Recent studies on resilience and system-operation also indicate that there are several high-impact disturbance mechanisms that are exposed to distribution systems. Hu et al. [16] studied resilience-enhancing strategies of distribution systems to endogenous wildfires, which suggests the general significance of protection planning during extreme events. Though their scope is the resilience of wildfire-related systems, and not lightning, the study still supports the necessity of system-level assessment techniques that could be used to quantify the effectiveness of risk and protection.

Normal and emergency operating modes of industrial power supply system have also been studied using computer modeling. Simulation was proven to be useful by Semenova et al. [17] when it comes to evaluating the behavior of power supply under abnormal conditions. This justifies the approach of modeling transient and protection behavior using MATLAB/Simulink based modeling before practically implementing it.

The overvoltage of lightning over the ground and soil is still of interest in the study of lightning overvoltage. Grange et al. [18] examined how stratified soil structures affect the indirect lightning-induced overvoltages in high- and medium-voltage overhead lines. Their experiment substantiates the fact that the properties of grounding and soil may have a powerful impact on the induced overvoltage levels. Tang et al. [19] also examined the optimization of reliability of distribution systems, demonstrating that the reliability of the networks is dependent on the coordinated design and operating conditions. In 220 kV transmission lines, Sanchez et al. [20] examined lightning-induced faults and protection malfunctions, and found that lightning can cause serious protection issues even in high-voltage transmission lines. Lastly, Qiu et al. [21] examined the improvement measures to lightning stroke breaking of 10 kV overhead insulated conductors, and the practical significance of enhancing the lightning protection in distribution networks.

In general, the literature indicates that the analysis of overvoltage caused by lightning should consider the induced voltage mechanisms, the effects of grounding, the performance of arrester, the stress on insulation, and the protection behavior of a system. Nevertheless, there are numerous works that concentrate on personal issues like the calculation of induced voltage, simulation of arrester, grounding, or fault detection. The current research paper fills this gap by incorporating three-phase feeder coupling, transformer surge transfer, nonlinear MOV arrester behavior, rise in grounding voltages, and flashover detection into a single MATLAB/Simulink-based protection system.

3. Mathematical Modeling and Algorithm Formulation

The main transient elements of a distribution feeder protection system have been combined to develop the proposed lightning protection model, which consists of the lightning source, matrix-coupled three-phase feeder, transformer surge transfer, nonlinear MOV surge arrester, grounding impedance, and flashover detection. The model allows the direct excitation of lightning surge excitation, and the indirect coupling of voltage through lightning coupling.

A double-exponential waveform was used to represent the direct lightning surge voltage:

$$v_L(t) = V_p\left(e^{-\alpha t} - e^{-\beta t}\right) \quad (1)$$

where $v_L(t)$is the lightning surge voltage, $V_p$is the selected peak surge magnitude, and α and β are the tail and front shaping coefficients. For indirect lightning, the feeder disturbance was represented as an induced voltage caused by nearby lightning current coupling:

$$v_{ind}(t) = M\frac{di_L(t)}{dt} \quad (2)$$

where $M$is the coupling coefficient and $i_L(t)$is the lightning current. The lightning current was similarly represented by a double-exponential function:

$$i_L(t) = I_p\left(e^{-\alpha_i t} - e^{-\beta_i t}\right) \quad (3)$$

where $I_p$is the lightning current peak, and $\alpha_i$and $\beta_i$define the current waveform shape.

The feeder was modeled using a second-order RLC transfer function:

$$H_f(s) = \frac{V_{out}(s)}{V_{in}(s)} = \frac{1}{LCs^2+RCs+} \quad (4)$$

In the implemented model, this became:

$$H_f(s) = \frac{1}{1.0\times10^{-9}s^2+2.5\times10^{-6}s+1} \quad (5)$$

The corresponding time-domain expression is:

$$1.0\times10^{-9}\frac{d^2v_o(t)}{dt^2} + 2.5\times10^{-6}\frac{dv_o(t)}{dt} + v_o(t) = v_i(t) \quad (6)$$

where $v_i(t)$and $v_o(t)$are the feeder input and output voltages.

To represent phase-to-phase interaction, the three-phase feeder was modeled using a matrix-based coupling formulation:

$$\mathrm{v}_{abc}(t) = \mathrm{K}_{phase}\mathrm{v}_{L,abc}(t) \quad (7)$$

with

$$\mathrm{K}_{phase} = \begin{bmatrix} 1.00 & 0.15 & 0.10 \\ 0.15 & 1.00 & 0.12 \\ 0.10 & 0.12 & 1.00 \end{bmatrix} \quad (8)$$

For a surge applied only to Phase A, the coupled phase voltages are:

$$v_A(t) = 1.00v_L(t), v_B(t) = 0.15v_L(t), v_C(t) = 0.10v_L(t) \quad (9)$$

Each coupled phase voltage is then passed through the feeder transfer function:

$$V_A(s) = H_f(s)V_{A,c}(s), V_B(s) = H_f(s)V_{B,c}(s), V_C(s) = H_f(s)V_{C,c}(s) \quad (10)$$

The transformer was modeled using a voltage ratio and a second-order transient transfer function:

$$H_T(s) = \frac{V_s(s)}{V_p(s)} = \frac{k_T}{a_Ts^2+b_Ts+1} \quad (11)$$

The implemented transformer model was:

$$H_T(s) = \frac{0.03773}{5.0\times10^{-11}s^2+5.0\times10^{-8}s+1} \quad (12)$$

where $V_p(s)$and $V_s(s)$are the transformer primary and secondary voltages, respectively. The enhanced transformer response was represented as:

$$v_{s,en}(t) = f_T\left(v_{s,ideal}(t), K_c, V_{sat,core}\right) \quad (13)$$

where $K_c = 0.005$is the transformer coupling coefficient and $V_{sat,core} = 2000$ Vis the core saturation reference level.

The MOV surge arrester was represented as a nonlinear voltage-current device. Although MOV behavior can generally be written as

$$I_{MOV} = kV_{MOV}^{\alpha} \quad (14)$$

the implemented model used a manufacturer-based nonlinear characteristic:

$$I_{MOV} = f_{MOV}(V_{MOV}) \quad (15)$$

The MOV-protected voltage was calculated as:

$$V_{protected}(t) = V_{in}(t) - Z_sI_{MOV}(t) \quad (16)$$

with current limiting given by:

$$I_{MOV}(t) = \min(f_{MOV}(V_{MOV}), I_{max}) \quad (17)$$

where $I_{max} = 40$ kA. The instantaneous MOV power indicator and approximate energy indicator were calculated as:

$$P_{MOV}(t) = | V_{MOV}(t)I_{MOV}(t) | \quad (18)$$

$$E_{MOV} = \int_0^{T_{sim}} | V_{MOV}(t)I_{MOV}(t) | dt \quad (19)$$

The grounding system was modeled as a resistance-inductance branch. The ground voltage rise is:

$$v_g(t) = R_gi_g(t) + L_g\frac{di_g(t)}{dt} \quad (20)$$

Since the grounding current is approximated by the MOV current,

$$i_g(t) \approx I_{MOV}(t) \quad (21)$$

the grounding voltage rise becomes:

$$v_g(t) = R_g I_{MOV}(t) + L_g \frac{dI_{MOV}(t)}{dt} \quad (22)$$

The final equipment voltage was then obtained as:

$$v_{eq}(t) = v_{protected}(t) + v_g(t) \quad (23)$$

Flashover was evaluated by comparing the final equipment voltage with the selected insulation threshold. The insulation margin is:

$$M_{ins}(t) = V_{flashover} - | v_{eq}(t) | \quad (24)$$

and the minimum insulation margin is:

$$M_{min} = \min_t \left(V_{flashover} - | v_{eq}(t) | \right) \quad (25)$$

The flashover indicator is defined as:

$$F(t) = \begin{cases} 1, & | v_{eq}(t) | \geq V_{flashover} \\ 0, & | v_{eq}(t) | < V_{flashover} \end{cases} \quad (26)$$

The overall flashover status for a simulation case is:

$$F_{case} = \max_t F(t) \quad (27)$$

Thus, $F_{case} = 1$indicates flashover occurrence, while $F_{case} = 0$indicates no flashover.

The complete direct-surge protection chain is represented as:

$$v_L(t) \rightarrow \mathrm{K}_{phase} \rightarrow H_f(s) \rightarrow H_T(s) \rightarrow f_{MOV} \rightarrow (R_g, L_g) \rightarrow v_{eq}(t) \rightarrow F_{case} \quad (28)$$

For indirect lightning, the input source is replaced by the induced-voltage formulation:

$$i_L(t) \rightarrow M \frac{di_L(t)}{dt} \rightarrow \mathrm{K}_{phase} \rightarrow H_f(s) \rightarrow H_T(s) \rightarrow f_{MOV} \rightarrow (R_g, L_g) \rightarrow v_{eq}(t) \rightarrow F_{case} \quad (29)$$

The main performance indices were calculated using peak values of the simulated waveforms:

$$V_{peak} = \max_t | v(t) | \quad (30)$$

$$I_{MOV,peak} = \max_t | I_{MOV}(t) | \quad (31)$$

$$V_{g,peak} = \max_t | v_g(t) | \quad (32)$$

$$V_{eq,peak} = \max_t | v_{eq}(t) | \quad (33)$$

The voltage reduction of the protection model was calculated as:

$$\eta = \frac{V_{unprotected,peak} - V_{protected,peak}}{V_{unprotected,peak}} \times 100 \quad (34)$$

For the advanced model comparison, the reduction relative to the basic unprotected feeder model was calculated as:

$$\eta_{adv} = \frac{V_{basic,peak} - V_{eq,peak}}{V_{basic,peak}} \times 100 \quad (35)$$

The overall simulation algorithm involves initializing the feeder, transformer, arrester, grounding, coupling, and flashover parameters; choosing either the direct or indirect lightning source mode; generating the corresponding surge waveform; applying the three-phase coupling matrix; passing the coupled voltages through the feeder and transformer models; using the nonlinear MOV arrester model; calculating the grounding voltage rise and final equipment voltage; evaluating insulation margin and flashover status; and repeating the procedure to all direct surge, indirect lightning, grounding resistance, and flashover threshold cases. This combined formulation allows the simple unprotected feeder response and the complex protected equipment response to be juxtaposed within the same simulation framework.

4. Methodology

This paper will use a simulation-based approach to assess the overvoltage propagation and protection of a distribution feeder system due to lightning. The proposed model was created in MATLAB/Simulink, in a staged modeling process, starting with a simple RLC feeder and gradually extending it into an integrated three-phase lightning protection model. The last model includes phase coupling of the matrices, transformer surge transfer, nonlinear MOV arrester behavior, grounding impedance, indirect lightning coupling and flashover detection.

The methodology will assess both component and system level response to direct and indirect lightning disturbances. Direct surge cases are used to study the behavior of feeder and protection-chain with controlled conditions of voltage impulse nearby, and indirect lightning cases are used to study the effects of nearby-induced voltage impulse on feeder and protection-chain behavior. The variation of grounding resistance and flashover threshold are also presented to determine the sensitivity of the system under protection to realistic design parameters. Primary simulation outputs are feeder voltage, transformer secondary voltage, MOV-protected voltage, MOV current, ground voltage rise, final equipment voltage, insulation margin and flashover status.

4.1 Simulation-Based Research Framework

The research strategy is founded on progressive simulation strategy where the lightning protection model is built on a simplified baseline feeder into a complete integrated protection system. The basic model involves one-phase RLC feeder to determine the unprotected overvoltage response. This model is further extended with representation of three-phase feeder, three phase phase coupling through matrices, transformer surge transfer, nonlinear MOV arrester behaviour, grounding impedance, indirect lightning coupling and flashover detectors. The new physical mechanism that is introduced with each stage is needed to model the surge propagation and protection performance in a more realistic way.

The simulation working process starts with the initiation of feeder, transformer, arrester, grounding, lightning, coupling, and flashover settings. Then a lightning disturbance is chosen as a direct voltage surge or an indirectly induced voltage due to the nearby lightning current. The disturbance is coupled to the three phase feeder, transferred through the transformer, limited by the MOV arrester and added to the grounding voltage

rise to achieve the final equipment voltage. The equipment final voltage is then compared with the threshold of the insulation withstand threshold to determine the insulation margin and flashover condition. This structure will allow a systematic comparison between the simplistic unprotected feeder response and the sophisticated system response. It is also used to parametrically evaluate the effects of varying direct surge magnitude, indirect lightning coupling strength, grounding resistance, and flashover threshold. Thus, the suggested framework represents a systematic foundation of the evaluation of the electrical stress caused by lightning, as well as the efficiency of the integrated protection system.

4.2 Proposed Lightning Protection System Architecture

The proposed lightning protection system is designed as a combined surge-propagation and protection chain of a three-phase distribution feeder. The architecture starts with a lightning disturbance source that can operate in two possible modes: a direct voltage surge applied to the feeder, or an indirectly induced voltage generated by the nearby lightning current coupling. This dual-source design enables the use of a single model to consider both the direct and nearby lightning effects.

Once the lightning disturbance is created, it is delivered to a three-phase feeder coupling stage based on a matrix. This step allocates the disturbance between phases A, B, C based on the phase-coupling matrix. The coupled phase voltages are then imposed on RLC feeder branches to get the transient response of each phase. This enables the feeder to be modeled as a coupled three-phase system as opposed to being represented as an isolated single conductor.

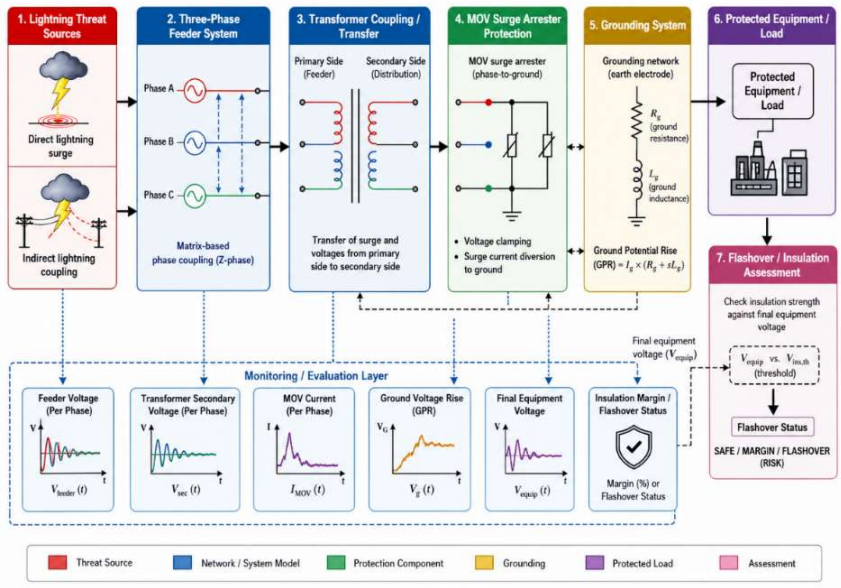

Figure 1. Conceptual framework of the proposed lightning protection system architecture.

Figure 1 transfers the feeder output through a transformer model, to estimate the surge voltage at the secondary side. Transformer block is a symbol of the voltage ratio as well as the transient transfer behavior between the primary and secondary sides. The surge voltage at the secondary side is then fed to the nonlinear MOV surge arrester model. The arrester limits overvoltage by conducting surge current when the voltage enters the arrester operating region, and thereby providing both an arrester current response and a clamped voltage response.

The arrester current is injected into the grounding system which is represented by resistance and inductance. Such grounding impedance generates rise in ground voltages during arrester conduction. The end equipment voltage is determined by adding the MOV-protected voltage to the rise in the ground voltage. This is required due to the fact that the grounding system could raise the overall insulation stress despite the fact that the local protected voltage is limited by the MOV arrester.

Lastly, the architecture has a block of flashover detection. This block compares the actual equipment voltage with the insulation withstand threshold selected and calculates the insulation margin corresponding to the selected insulation withstand threshold. When the end equipment voltage is greater than the threshold, the flashover is recorded. The suggested architecture thus considers not just the reduction of voltages but also the insulation risk at the equipment level.

4.3 Development of the Integrated MATLAB/Simulink Model

The integrated MATLAB/Simulink model has been created by integrating the respective subsystem models into one lightning surge protection platform. The model is a full temporary route of the lightning disturbance source to the terminal of the protected equipment. It encompasses the selection of source mode, three-phase feeder coupling that is matrix-based, feeder transfer response, transformer surge transfer, nonlinear MOV

arrester behavior, grounding voltage rise and flashover detecting.

A modelling style that was embraced was modular such that each subsystem could be developed and tested individually and then integrated. Feeder was initially modeled with branches of transfer functions based on the RLC. This single phase model was then extended into a three phase feeder and a coupling matrix was then introduced to represent the phase to phase interaction during transient events. This enabled the model to reflect the unequal distribution of the surge voltage between the phases A, B and C.

The subsystem of the transformer was attached following the feeder stage in order to calculate the surge voltage at the secondary side. This MOV arrester subsystem was then coupled at the secondary side to simulate nonlinear voltage clamping and arrester current conduction. The arrester current was taken as the input of the grounding branch where grounding resistance and inductance were used to calculate the rise in the ground voltage.

The voltage of the final equipment was calculated by summing the voltage across MOV and the voltage rise across ground. This was then compared to the selected insulation threshold by adding a flashover detection block. The block generates the insulation margin and binary flashover status of each of the simulation cases.

A source-mode selection mechanism is also a part of the integrated model. Direct surge mode involves a controlled voltage impulse being applied to the feeder. In indirect lightning mode, one of the coupling coefficients is chosen to transform a local lightning current into an induced feeder voltage. This design enables the direct and indirect cases of lightning to be considered in the same Simulink model.

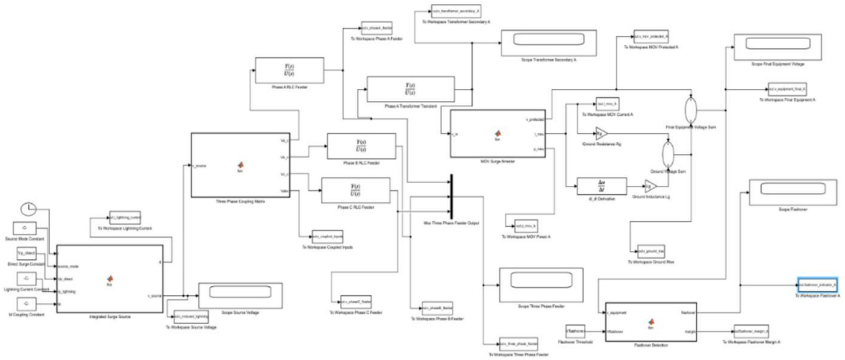

Figure 2. Integrated MATLAB/Simulink model architecture for lightning surge analysis.

The entire Simulink implementation, including the selection of the source, the three-phase feeder connection, the transformer, the MOV arrester, the grounding branch, and the flashover detection are shown in the figure

4.4 Lightning Disturbance and Test Scenario Formulation

The scenarios of the lightning disturbance were designed to test the proposed model in the direct and indirect overvoltage mechanisms. A controlled voltage impulse is impressed on the feeder input to directly represent direct lightning-induced overvoltage stress. The mode is employed to examine how increasing the magnitude of the surge propagates through the feeder, transformer, MOV arrester, grounding system and the terminal of the protected equipment.

In the case of the direct surge study the applied voltage peak was varied over a wide range to represent moderate, severe and extreme feeder stress conditions:

$$V_p = \{20,\ 50,\ 100,\ 200,\ 500,\ 1000\}\ \text{kV}$$

where $V_p$is the peak value of the applied surge voltage. The 1 MV case was added as a highly sensitive case of the upper stress response of the integrated protection chain. The value of 300 MV of natural lightning potential was not entered as a normal input of a direct feeder but was instead considered separately as an extreme theoretical induced-voltage demonstration.

In indirect lightning mode, the disturbance in the feeder is induced by the near lightning current via electromagnetic coupling. The induced voltage is related to the change of lightning current rate and the coupling coefficient. The indirect lightning cases were characterized by a combination of different values of both the lightning current peak and coupling coefficient:

$$I_p = \{10,\ 30,\ 50,\ 100\}\ \text{kA}$$

$$M = \{2,\ 10,\ 20,\ 50\}\mu\text{H}$$

where $I_p$is the lightning current peak and $M$is the coupling coefficient between the lightning channel and feeder.

Additional sensitivity scenarios were used to evaluate grounding and insulation effects. The grounding resistance was varied as:

$$R_g = \{0.1,\ 0.5,\ 1,\ 2,\ 5,\ 10\}\Omega$$

while the grounding inductance was kept constant. The flashover threshold was varied as:

$$V_{\text{flashover}} = \{25,\ 35,\ 50,\ 75,\ 100\}\ \text{kV}$$

These scenario groups provide a structured basis for evaluating direct surge severity, indirect lightning coupling, grounding degradation, and insulation withstand sensitivity within the same simulation framework.

4.5 Protection Component Modeling Strategy

The protection elements were modelled to reflect the key processes that influence the lightning surge propagation

and mitigation in the distribution feeder. The transformer was modeled as a surge-transfer element between the feeder primary side and the protected secondary side, both in terms of the transformation ratio of the voltages and the transient response.

The MOV surge arrester was a nonlinear protective element that was modeled as a voltage-current characteristic, instead of fixed saturation limit. This enabled the model to be used to estimate the clamped voltage and arrester current during surge events. Resistance and inductance were used to model the grounding system to capture the rise in ground voltages due to the discharge current in arrester.

The flashover detection was done based on threshold-based insulation model. The equipment voltage at the final equipment was compared to the chosen flashover threshold to calculate the insulation margin and flashover condition. This component modeling strategy, in general, is a combination of transformer attenuation, MOV clamping, grounding voltage rise, and insulation withstand assessment into a single protection chain.

4.6 Numerical Simulation Protocol

All simulations were performed in MATLAB/Simulink using a fixed-step numerical procedure to capture fast lightning-induced transient behavior. The integrated model was solved using the fourth-order Runge–Kutta solver, ode4, with a fixed step size of:

1×10^{-6} s

This time step was chosen to give sufficient resolution to steep-front surge waveforms, MOV conduction intervals, rise in grounding voltage, and flashover detection.

The parameters of the feeder, transformer, MOV arrester, grounding, coupling, and flashover were set up in the MATLAB workspace before each run of the simulation. The selected case variables such as the magnitude of the direct surge, peak of the lightning current, coupling coefficient, grounding resistance and flashover threshold were then assigned to the workspace and were passed to the Simulink model. This enabled the same integrated model to be re-used in all the scenario groups.

In each case, the output signals were sent out of Simulink to MATLAB workspace. These were the lightning source voltage, coupled phase input voltages, feeder phase voltages, transformer secondary voltage, MOV-protected voltage, MOV current, ground voltage rise, final equipment voltage, flashover margin and flashover indicator. Peak values, insulation margin, MOV energy indicator and flashover status were calculated using these signals.

The simulation process was done systematically to all the pre-defined groups of scenarios. Direct surge cases were evaluated as increasing voltage stress, indirect lightning cases were evaluated as current-coupling effects, grounding cases were evaluated as the influence of grounding resistance and flashover-threshold cases were evaluated as the sensitivity of insulation withstand. This guaranteed similar numerical settings and model structure in all simulations.

4.7 Performance Evaluation Criteria

The lightning protection model proposed was tested with the help of the main electrical stress and protection indicators along the surge propagation path. These were peak feeder voltage, transformer secondary voltage, MOV-protected voltage, peak MOV current, MOV energy indicator, rise in ground voltage, final equipment voltage, insulation margin and flashover status.

The unprotected baseline response was the peak feeder voltage and the transformer secondary voltage indicated the amount of surge transferred to the protected side. The performance of MOV was evaluated by the use of the clamped voltage, arrester current and energy indicator. The grounding performance was measured by the increase in peak ground voltage and the end equipment voltage was considered as the primary system-level stressor.

The minimum insulation margin and binary flashover status were used to assess the safety of insulation. A positive margin is that the insulation threshold has not been crossed, whilst a negative margin indicates that the insulation threshold has been surpassed. Lastly, the advanced model was compared with the basic feeder model by computing the decrease in final equipment voltage in comparison to the unprotected feeder voltage.

5. Results

5.1. Matrix-Coupled Three-Phase Feeder Response

The three-phase feeder response with a matrix-coupled was tested in a surge that was added to Phase A. Phase A generates the largest transient response, with Phases B and C generating smaller coupled voltages because of the off-diagonal terms of the phase-coupling matrix.

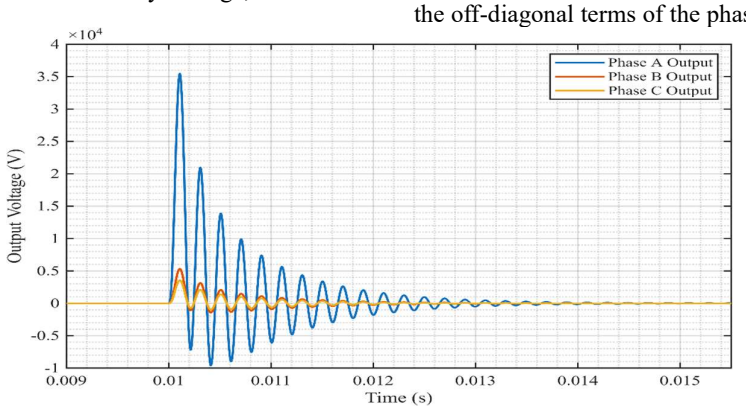

Figure 3. Matrix-coupled three-phase feeder response under Phase-A lightning surge excitation.

The figure indicates that the Phase-A bursts cause smaller yet significant transient effects in Phases B and C.
This behavior is confirmed by the peak values in Table 1. Phase A takes the entire input of 20.00 kV and the output of the feeder is 35.47 kV. Phase B is coupled with 15% and generates a 3.00 kV input and 5.32 kV output. Phase C is coupled with 10% and generates a 2.00 kV input and 3.55 kV output.

Table 1. Matrix-based three-phase feeder coupling results.

Phase	Coupling from A	Input peak (kV)	Output peak (kV)
Phase A	1.000	20.00	35.47
Phase B	0.150	3.00	5.32
Phase C	0.100	2.00	3.55

The table summarizes the effective coupling of Phase A, the coupled input peak voltage and the resulting feeder output peak voltage of each phase.
These findings support the fact that the matrix-based feeder model is able to capture unequal distribution of surge among phases, which forms the basis of the subsequent transformer, MOV, grounding and flashover analysis.

5.2 Transformer Surge Transfer Response

The transformer surge transfer response was tested when the three-phase feeder output was applied to the primary side of the transformer. The transformer as illustrated in Fig. 4, minimizes the magnitude of the surge reaching the secondary side without altering the relative phase behavior, with Phase A prevailing.

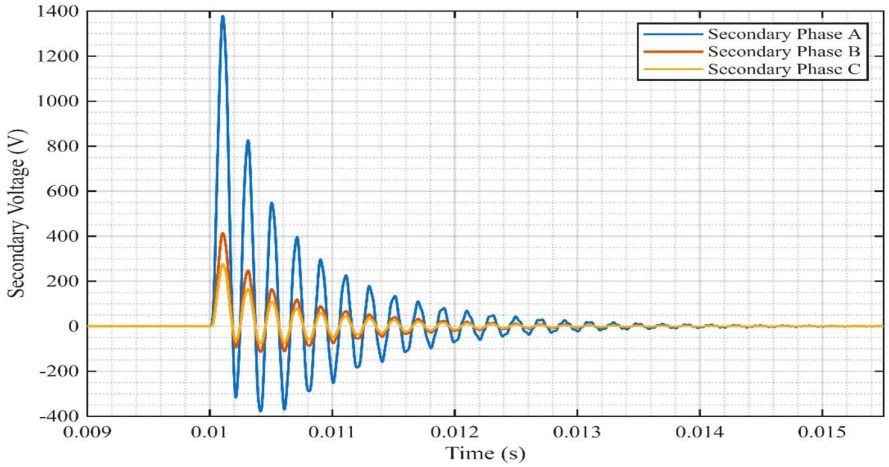

Figure 4. Transformer secondary surge response under three-phase feeder excitation.

The figure illustrates the lower secondary-side transient voltages of phases A, B and C following transformer surge transfer.
This decrease is supported by the numerical data in Table 2. Phase A reduces on the primary side (35.47 kV) to the secondary side (1.379 kV). Phase B decreases from 10.64 kV to 0.414 kV, while Phase C decreases from 7.09 kV to 0.276 kV.

Table 2. Transformer surge transfer results.

Phase	Coupling factor	Primary peak (kV)	Secondary peak (kV)
Phase A	1.000	35.47	1.379
Phase B	0.300	10.64	0.414
Phase C	0.200	7.09	0.276

These findings indicate that the transformer can greatly reduce the feeder-side surge, but the secondary-side transient still needs to be downstream-protected by the MOV arrester and grounding system.

5.3 Ideal and Enhanced Transformer Model Comparison

The optimal and improved transformer responses were compared to evaluate the impact of introducing simplified transformer dynamics in addition to scaling by voltage ratios. The improved transformer model, as illustrated in Fig. 5, alters the waveform at the secondary side, by adding coupling and saturation-related behavior.

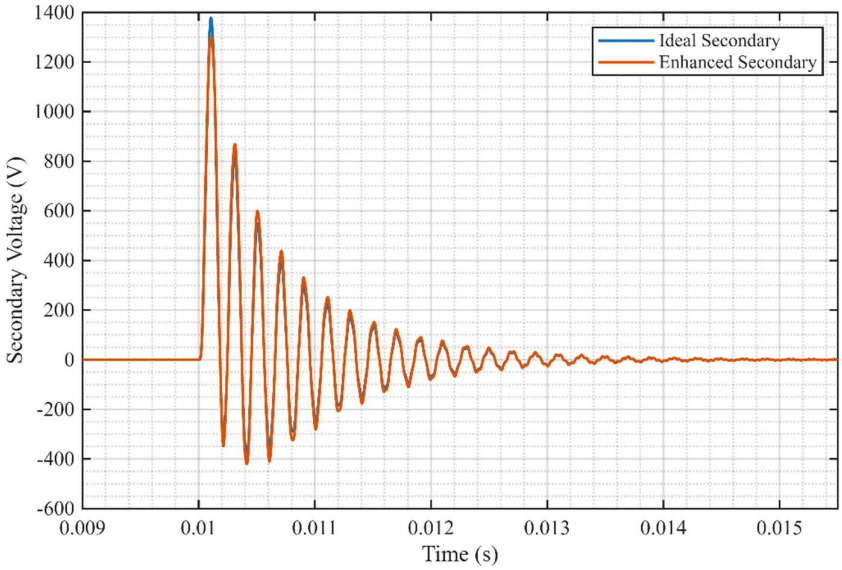

Figure 5. Ideal versus enhanced transformer secondary response under lightning surge excitation.

The figure contrasts the ideal secondary response with the improved transformer response, and demonstrates the impact of non-ideal transformer behavior during surge transfer.

The numerical results in Table 3 indicate that Phase A reduces to an ideal secondary peak of 1.379 kV to an enhanced value of 1.303 kV. In Phase B, the enhanced value rises by 0.414 kV to 0.458 kV, whereas, in Phase C, the enhanced value increases by 0.276 kV to 0.309 kV.

Table 3. Ideal and enhanced transformer comparison results.

Phase	**Coupling factor**	**Primary peak (kV)**	**Ideal secondary (kV)**	**Enhanced secondary (kV)**
Phase A	1.000	35.47	1.379	1.303
Phase B	0.300	10.64	0.414	0.458
Phase C	0.200	7.09	0.276	0.309

These findings indicate that the improved transformer model does not merely scale the primary voltage evenly, it alters the secondary response based on the additional transformer dynamics. This enhances physical realism of the subsequent integrated protection-chain simulation.

5.4 MOV Surge Arrester Voltage-Clamping Performance

The nonlinear MOV surge arrester voltage-clamping performance was measured by comparing the unprotected and MOV-protected output voltages. The MOV arrester (Fig. 6) limits the transient peak when it enters its conducting region, thus reducing the voltage applied to the protected terminal.

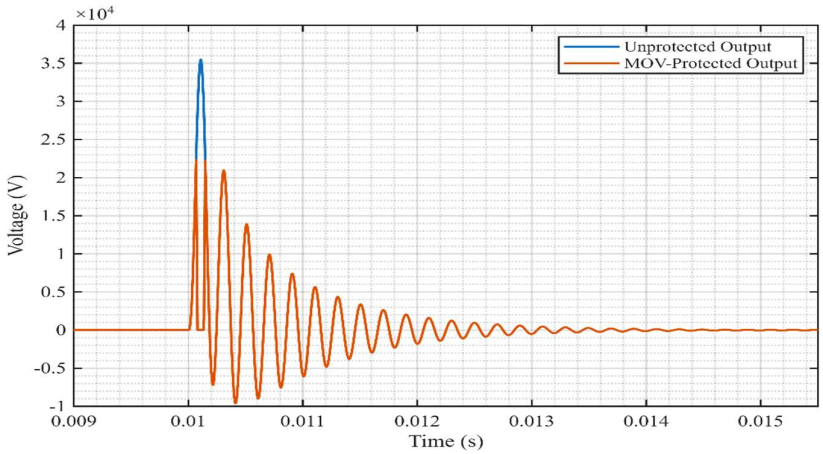

Figure 6. MOV-protected versus unprotected voltage response under lightning surge excitation.

The figure compares the unprotected output voltage with the MOV-protected voltage, and illustrates the voltage-limiting effect of the nonlinear arrester model.
Table 4 results indicate that the unprotected output is 35.47 kV when the input surge is 20.00 kV, and the MOV-protected output is lower (22.34 kV) than the unprotected output (35.47 kV). This will provide a voltage drop of 37.00%.

Table 4. MOV voltage-clamping performance results.

Input peak (kV)	Unprotected peak (kV)	MOV-protected peak (kV)	Voltage reduction (%)
20.00	35.47	22.34	37.00

These findings validate the fact that the MOV arrester offers effective voltage limiting, but the voltage that is limited is not totally suppressed. The stresses of arrester current and energy are thus discussed next.

5.5 MOV Arrester Current and Energy Stress

The MOV arrester current and energy stress were measured to determine the level of discharge when voltage clamping is applied. The MOV current increases rapidly when the surge voltage reaches the arrester operating region, indicating active diversion of surge-current.

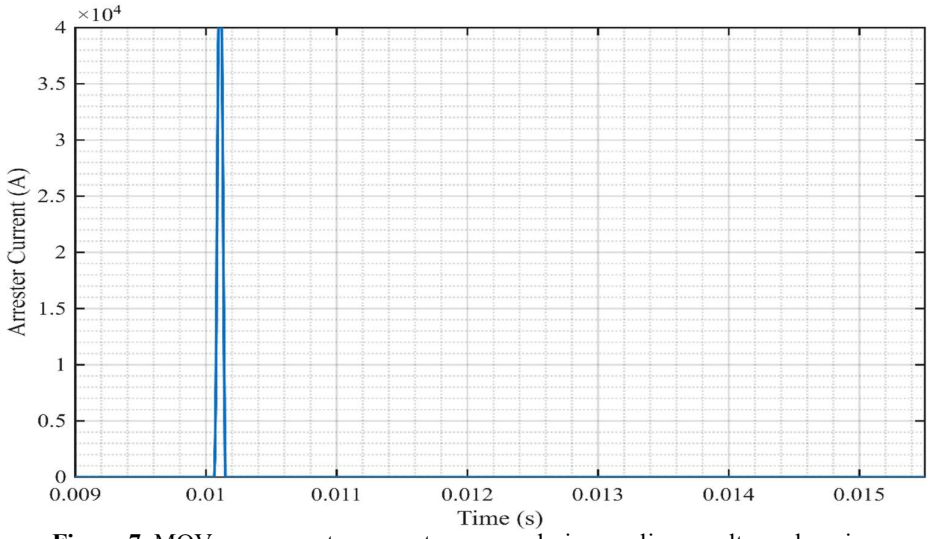

Figure 7. MOV surge arrester current response during nonlinear voltage clamping.

The figure indicates the momentary current that the MOV arrester carries during the surge event.
Table 5 presents the numerical results that indicate that the MOV current is 40,000 A. The peak power indicator is about 8.326 x 107 W and the approximate energy indicator is 1398.01 J.

Table 5. MOV arrester current and energy indicator results.

MOV current peak (A)	MOV power indicator peak (W)	MOV energy indicator (J)
40000	8.326×10^7	1398.01

These findings indicate that MOV performance needs to be assessed based on both voltage-clamping capacity and discharge stress. The arrester must be able to sustain a high current and energy when conducting a surge, though it will reduce the voltage being protected.

5.6 Grounding System Response and Ground Voltage Rise

The response of the grounding system was tested in the conduction of MOV arrester to understand how discharge current results in ground voltage rise. Fig. 8 shows that the ground voltage increases during the MOV conduction interval, which means that the grounding branch does not act as an ideal zero-potential reference in the discharge of surge currents.

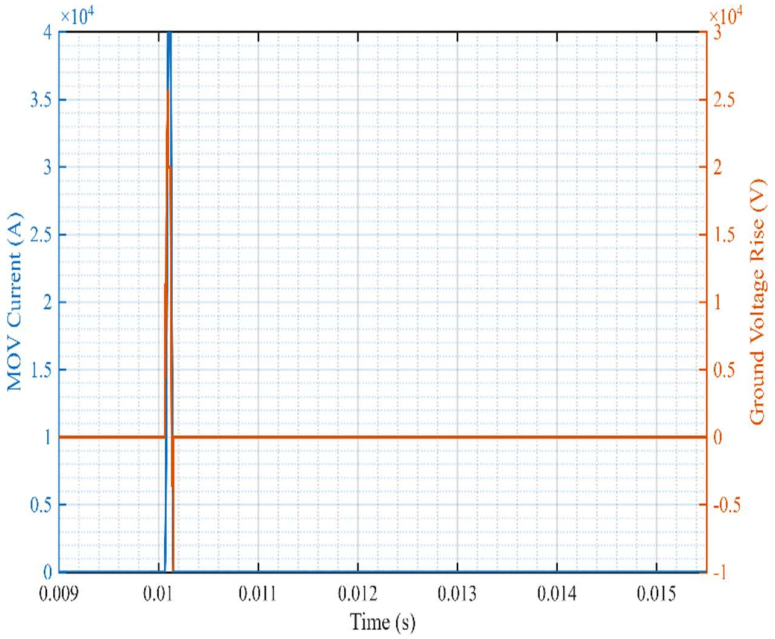

Figure 8. Ground voltage rise response during MOV arrester discharge.

The figure is a transient increase in ground voltage caused when the current of MOV arrester flows through the grounding impedance.

The Table 6 results indicate that, at 20.00 kV input surge, the voltage across the MOV is 22.34 kV and the current flowing through the MOV is 40,000 A. The grounding system causes an increase in the ground voltage of the final equipment to 30.11 kV. Consequently, the reduction in the case of MOV-only protection is reduced to 15.12% with the consideration of the grounding effects.

Table 6. Grounding system voltage-rise results.

Input peak (kV)	MOV-protected peak (kV)	MOV current (A)	Ground rise (kV)	Final equipment peak (kV)	MOV-only reduction (%)	Reduction with ground (%)
20.00	22.34	40000	25.66	30.11	37.00	15.12

These findings demonstrate that grounding voltage rise can be a major contributor to the eventual equipment voltage, even when the MOV arrester is able to effectively clamp the local protected voltage. Thus, grounding should be considered along with arrester performance.

5.7 Grounding Resistance Sensitivity

The sensitivity of grounding resistance was examined in order to find out the impact of the quality of grounding on the ground voltage rise and the final equipment voltage. Fig. 9 shows that both quantities increase with an increase in R_g increases the voltage drop across a higher grounding impedance.

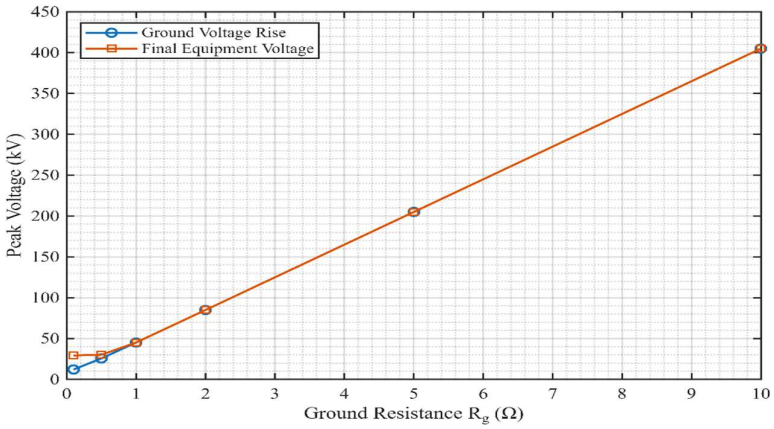

Figure 9. Ground resistance sensitivity of ground voltage rise and final equipment voltage.

The figure indicates that the poor grounding conditions are major contributors to the voltage stress that is imposed on the equipment that is being provided protection.
This trend is confirmed by the numerical results in Table 7. The last equipment voltage is 29.28 kV when the value of Rg equals 0.10 Ω. At R g=0.50 -1, it is still lower than the 35 kV reference level at 30.11 kV. Nonetheless, as Rgincreases to 1.00 Ω, the final equipment voltage r increases to 45.16 kV which is above the reference threshold. At R_g=10 Ω, the final equipment voltage reaches 404.95 kV.

Table 7. Grounding resistance sensitivity results.

Rg (Ω)	Input peak (kV)	MOV-protected peak (kV)	Ground rise (kV)	Final equipment peak (kV)	Reduction with ground (%)
0.10	20.00	22.34	12.13	29.28	17.44
0.50	20.00	22.34	25.66	30.11	15.12
1.00	20.00	22.34	45.16	45.16	-27.34
2.00	20.00	22.34	84.95	84.95	-139.53
5.00	20.00	22.34	204.95	204.95	-477.88
10.00	20.00	22.34	404.95	404.95	-1041.79

These results show that grounding resistance is a dominant factor in final equipment stress. Low grounding resistance limits ground voltage rise, whereas high resistance can make the final equipment voltage exceed the MOV-protected voltage and the insulation reference level.

5.8 Indirect Lightning Coupling Response

The response of indirect lightning coupling was assessed to evaluate the influence of the coupling coefficient *M* on the induced feeder voltage and protection operation. The induced voltage increases with *M* as shown in Fig. 10, and at low coupling values the MOV does not conduct and at the highest coupling value the induced voltage is sufficient to activate MOV clamping and grounding discharge.

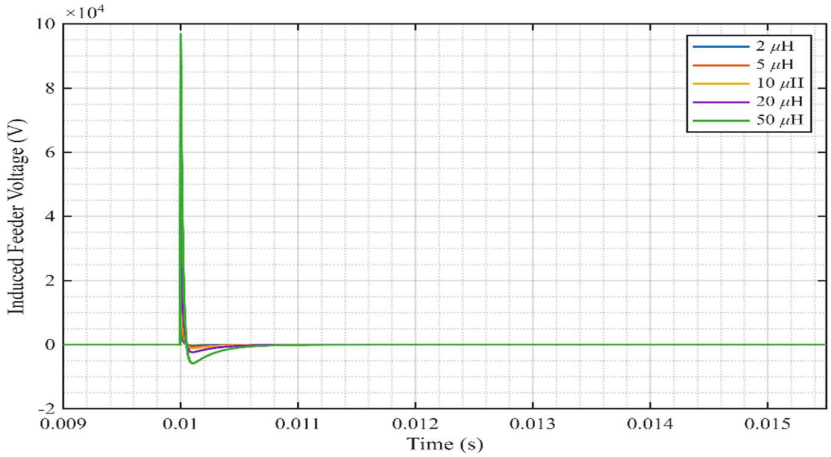

Figure 10. Indirect lightning coupling response under different coupling coefficients.

The figure indicates that greater electromagnetic coupling results in greater induced feeder voltage and can cause the MOV arrester to operate.
The table 8 results indicate that at M=2 µH, the induced voltage is 3.875 kV and the final equipment voltage is 1.919 kV. At M=20 µH, the induced voltage increases to 38.75 kV, but the MOV current has not changed, 0 A. At M=50 µH, the induced voltage is increased to 96.87 kV, but the MOV current has not changed, 0 A. At M=50 µH, the induced voltage has increased to 96.87 kV, but the MOV current has not changed, 0 A.

Table 8. Indirect lightning coupling-strength results.

M (µH)	Lightning current (kA)	Induced voltage (kV)	Unprotected peak (kV)	MOV-protected peak (kV)	MOV current (A)	Ground rise (kV)	Final equipment peak (kV)
2.00	30.00	3.875	1.919	1.919	0	0	1.919
5.00	30.00	9.687	4.798	4.798	0	0	4.798
10.00	30.00	19.37	9.595	9.595	0	0	9.595
20.00	30.00	38.75	19.19	19.19	0	0	19.19
50.00	30.00	96.87	47.98	22.38	40000	44.53	44.53

These findings indicate that indirect lightning is mild when the coupling is weak and severe when the coupling is strong. The grounding effects have a strong impact on the end equipment voltage once the MOV conducts.

5.9 Flashover and Insulation Margin Analysis

The flashover behavior was tested by comparing the final equipment voltage with various insulation withstand thresholds. As illustrated in Fig. 11, insulation margin gets higher with increase in flashover threshold. The negative values in the margin represent a flashover risk whereas positive values represent safe operation.

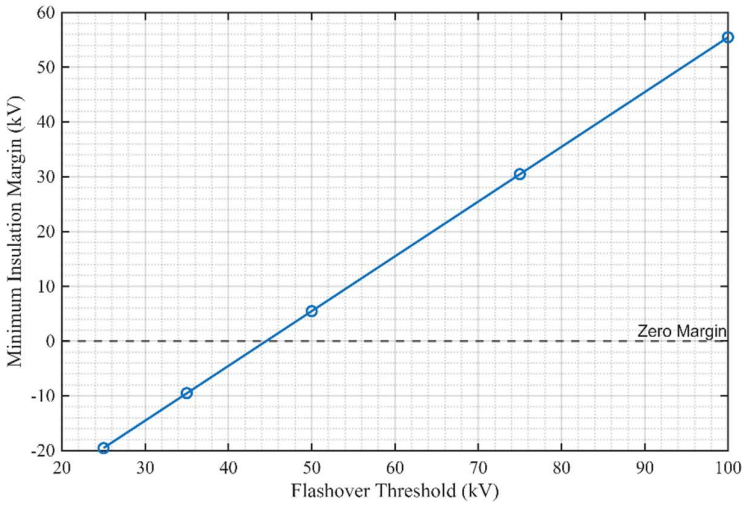

Figure 11. Flashover and insulation margin response under different insulation thresholds.

The figure shows the variation of minimum insulation margin with flashover threshold.
Table 9 results indicate that the final equipment voltage is 44.53 kV in the case of severe indirect lightning. The margins are -19.53 kV, and -9.53 kV, respectively, at thresholds of 25 kV and 35 kV, respectively, so flashover occurs. At a threshold of 50 kV, the margin is positive at 5.47 kV and flashover does not occur any longer.

Table 9. Flashover threshold and insulation margin results.

Threshold (kV)	Induced voltage (kV)	MOV-protected peak (kV)	Ground rise (kV)	Final equipment peak (kV)	Minimum margin (kV)	Flashover status	MOV current (A)	MOV energy (J)
25.00	96.87	22.38	44.53	44.53	-19.53	1	40000	8243.23
35.00	96.87	22.38	44.53	44.53	-9.53	1	40000	8243.23
50.00	96.87	22.38	44.53	44.53	5.47	0	40000	8243.23
75.00	96.87	22.38	44.53	44.53	30.47	0	40000	8243.23
100.00	96.87	22.38	44.53	44.53	55.47	0	40000	8243.23

The results of this experiment confirm that flashover is not only dependent on the final equipment voltage, but also on the voltage across the MOV. This test condition is that the transition between flashover and safe operation is between 35 kV and 50 kV.

5.10 Integrated Direct Surge Performance of the Advanced Model

The integrated direct surge response was tested with complete protection chain which includes feeder coupling, transformer transfer, MOV clamping, grounding rise and flashover detection. As Fig. 12 shows, the feeder voltage is increased by the applied direct surge and decreased by the transformer and MOV stages, respectively.

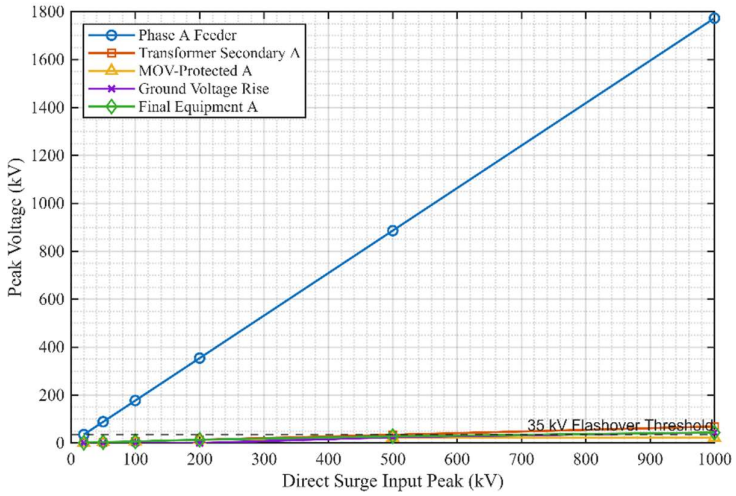

Figure 12. Integrated direct surge response through the advanced protection chain.

The figure compares the Phase A feeder voltage, transformer secondary voltage, MOV-protected voltage, rise in ground voltage, and final equipment voltage when there is a direct surge input between 20 kV and 1 MV.
The Table 10 results indicate that when the inputs are between 20 kV and 200 kV, the MOV current is 0 A, and there is no flashover. The MOV operates at 40,000 A at 500 kV and limits the voltage MOV-protected to 22.20 kV and gives a final equipment voltage of 28.28 kV. The last equipment voltage at 1 MV is 43.81 kV with a negative margin of -8.81 kV that results in flash over.

Table 10. Integrated direct surge case results.

Direct input (kV)	Phase A feeder (kV)	Transformer sec. A (kV)	MOV-protected A (kV)	MOV current A (A)	Ground rise (kV)	Final equipment A (kV)	Margin A (kV)	Flashover status	MOV energy A (J)
20.00	35.47	1.379	1.379	0	0	1.379	33.62	0	0
50.00	88.67	3.446	3.446	0	0	3.446	31.55	0	0
100.00	177.33	6.893	6.893	0	0	6.893	28.11	0	0
200.00	354.67	13.79	13.79	0	0	13.79	21.21	0	0
500.00	886.67	34.46	22.20	40000	24.49	28.28	6.72	0	1465.28
1000.00	1773.33	68.93	22.34	40000	43.81	43.81	-8.81	1	4483.15

These findings demonstrate that the integrated protection model is effective up to the 500 kV case of direct surge but the 1 MV case exceeds the insulation limit since the case has higher ground voltage rise.

5.11 Integrated Scenario Comparison

The integrated model was compared in direct surge, indirect lightning and extreme inducedvoltage conditions. The end equipment voltage, as in Fig. 13, is highly dependent on the source type and the severity of the disturbance. The 100 kV and 500 kV direct-to-ground surge cases are below the 35 kV direct current flashover point, and the 1 MV direct-to-ground surge and 300 MV induced demonstrations exceed the flashover point.

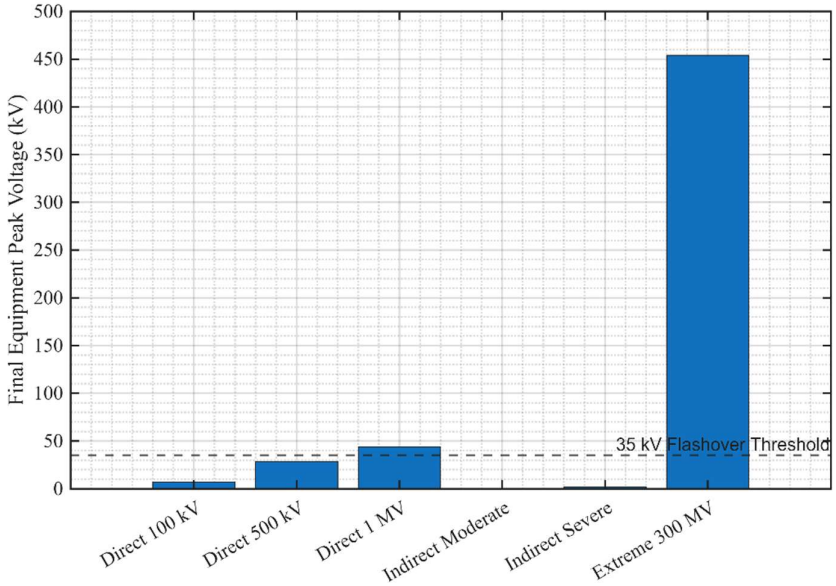

Figure 13. Integrated scenario comparison of final equipment voltage under direct and indirect lightning conditions.

The figure compares the final equipment voltage in direct surge, indirect lightning and extreme induced voltage conditions using the 35 kV flashover threshold as the reference level.

The Table 11 results indicate that the 100 kV direct surge results in a final equipment voltage of 6.893 kV, whereas the 500 kV case yields a final equipment voltage of 28.28 kV, after MOV clamping and grounding effects. In the case of 1 MV, the final equipment voltage increases to 43.81 kV which leads to flashover. The moderate and severe cases of indirect lightning are not high at 0.081 kV and 2.031 kV, respectively. Conversely, the demonstration with induced 300 MV has a final equipment voltage of 454.00 kV and negative margin of -419.00 kV.

Table 11. Integrated scenario comparison results.

Scenario	Mode	Source peak (kV)	Phase A feeder (kV)	Transformer sec. A (kV)	MOV-protected A (kV)	MOV current A (A)	Ground rise (kV)	Final equipment A (kV)	Margin A (kV)	Flashover status
Moderate Direct Surge 100 kV	1	100.00	177.33	6.893	6.893	0	0	6.893	28.11	0
Severe Direct Surge 500 kV	1	500.00	886.67	34.46	22.20	40000	24.49	28.28	6.72	0
Extreme Direct Surge 1 MV	1	1000.00	1773.33	68.93	22.34	40000	43.81	43.81	-8.81	1
Moderate Indirect Lightning	2	3.875	1.919	0.081	0.081	0	0	0.081	34.92	0
Severe Indirect Lightning	2	96.87	47.98	2.031	2.031	0	0	2.031	32.97	0
Extreme 300 MV Induced Demonstration	2	299995	148586	6290.53	34.00	40000	420.00	454.00	-419.00	1

These findings affirm that MOV clamping alone cannot be used to conduct insulation assessment. Equipment final voltage should be assessed with the addition of transformer transfer, MOV operation, grounding rise and flashover threshold.

5.12 Advanced Parametric Test-Case Evaluation

The developed parametric assessment looks at the combined model under direct surge, indirect lightning coupling, grounding resistance, and variations in flashover threshold. Final equipment voltage depends on type of disturbance and system parameters, with grounding resistance being the most influential.

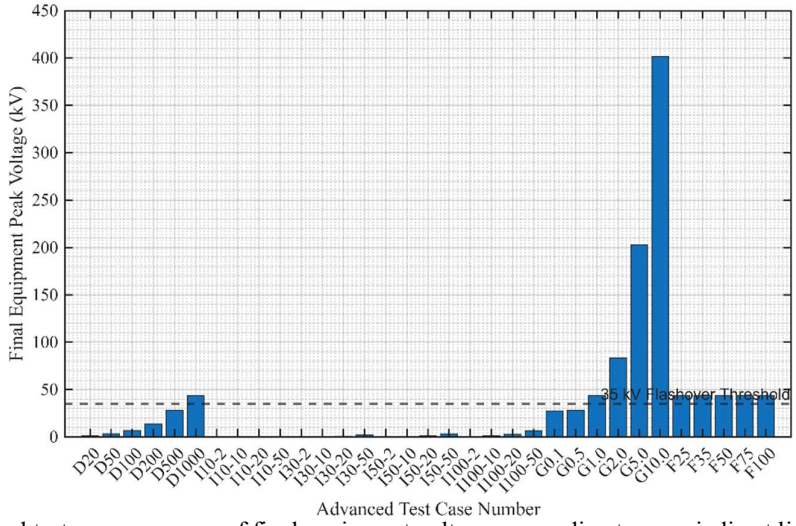

Figure 14. Advanced test-case summary of final equipment voltage across direct surge, indirect lightning, grounding, and flashover sensitivity cases.

The figure shows final equipment voltage to direct sweep of surge, indirect lightning coupling, sensitivity of grounding resistance and flashover threshold cases with a 35 kV reference limit.

The results of the direct surge sweep (Table 12) indicate that the final equipment voltage rises with the input of 1.379 kV (20 kV input) to 43.81 kV (1 MV input). MOV conduction starts at 500 kV, but does not prevent flashover at 1 MV..

Table 12. Direct surge sweep results.

Case	Direct input (kV)	Phase A feeder (kV)	Transformer sec. A (kV)	MOV-protected A (kV)	MOV current A (A)	Ground rise (kV)	Final equipment A (kV)	Flashover status
Direct surge 20 kV	20	35.47	1.379	1.379	0	0	1.379	0
Direct surge 50 kV	50	88.67	3.446	3.446	0	0	3.446	0
Direct surge 100 kV	100	177.33	6.893	6.893	0	0	6.893	0
Direct surge 200 kV	200	354.67	13.79	13.79	0	0	13.79	0
Direct surge 500 kV	500	886.67	34.46	22.20	40000	24.49	28.28	0
Direct surge 1000 kV	1000	1773.33	68.93	22.34	40000	43.81	43.81	1

The indirect lightning sweep (**Table 13**) shows that final equipment voltage remains below **6.8 kV** for all tested current–coupling combinations, and no flashover occurs.

Table 13. Indirect lightning current-coupling sweep results.

Ip (kA)	M (µH)	Source peak (kV)	Phase A feeder (kV)	Transformer sec. A (kV)	MOV-protected A (kV)	MOV current A (A)	Final equipment A (kV)	Flashover status
10.00	2.00	1.292	0.640	0.027	0.027	0	0.027	0
10.00	10.00	6.458	3.198	0.135	0.135	0	0.135	0
10.00	20.00	12.92	6.397	0.271	0.271	0	0.271	0
10.00	50.00	32.29	15.99	0.677	0.677	0	0.677	0
30.00	2.00	3.875	1.919	0.081	0.081	0	0.081	0
30.00	10.00	19.37	9.595	0.406	0.406	0	0.406	0
30.00	20.00	38.75	19.19	0.812	0.812	0	0.812	0
30.00	50.00	96.87	47.98	2.031	2.031	0	2.031	0
50.00	2.00	6.458	3.198	0.135	0.135	0	0.135	0
50.00	10.00	32.29	15.99	0.677	0.677	0	0.677	0
50.00	20.00	64.58	31.98	1.354	1.354	0	1.354	0
50.00	50.00	161.44	79.96	3.385	3.385	0	3.385	0
100.00	2.00	12.92	6.397	0.271	0.271	0	0.271	0
100.00	10.00	64.58	31.98	1.354	1.354	0	1.354	0
100.00	20.00	129.15	63.97	2.708	2.708	0	2.708	0
100.00	50.00	322.89	159.92	6.771	6.771	0	6.771	0

The grounding and flashover sensitivity (**Table 14**) confirms that increasing grounding resistance causes rapid voltage escalation and flashover beyond **1 Ω**, while higher insulation thresholds improve safety margins.

Table 14. Grounding and flashover sensitivity summary.

Sensitivity parameter	Parameter value	Direct input (kV)	Ground rise (kV)	Final equipment A (kV)	Margin A (kV)	Flashover status
Ground resistance	0.1 Ω	500	12.58	27.62	7.38	0
Ground resistance	0.5 Ω	500	24.49	28.28	6.72	0
Ground resistance	1 Ω	500	43.95	43.95	-8.95	1
Ground resistance	2 Ω	500	83.64	83.64	-48.64	1
Ground resistance	5 Ω	500	202.72	202.72	-167.72	1
Ground resistance	10 Ω	500	401.54	401.54	-366.54	1
Flashover threshold	25 kV	1000	43.81	43.81	-18.81	1
Flashover threshold	35 kV	1000	43.81	43.81	-8.81	1
Flashover threshold	50 kV	1000	43.81	43.81	6.19	0
Flashover threshold	75 kV	1000	43.81	43.81	31.19	0
Flashover threshold	100 kV	1000	43.81	43.81	56.19	0

In general, the findings confirm that the initial stress is determined by direct surge magnitude, indirect coupling is not particularly risky under test conditions, grounding resistance is the most important risk factor, and flashover is dependent on the relationship between final equipment voltage and insulation threshold.

5.13 Basic and Advanced Model Comparison

This part is a comparison of the simple unprotected feeder model and the sophisticated integrated protection model to measure the effectiveness of the entire protection chain. The advanced model, as illustrated in Fig. 15, can greatly lower the voltage to the equipment than with the basic feeder response.

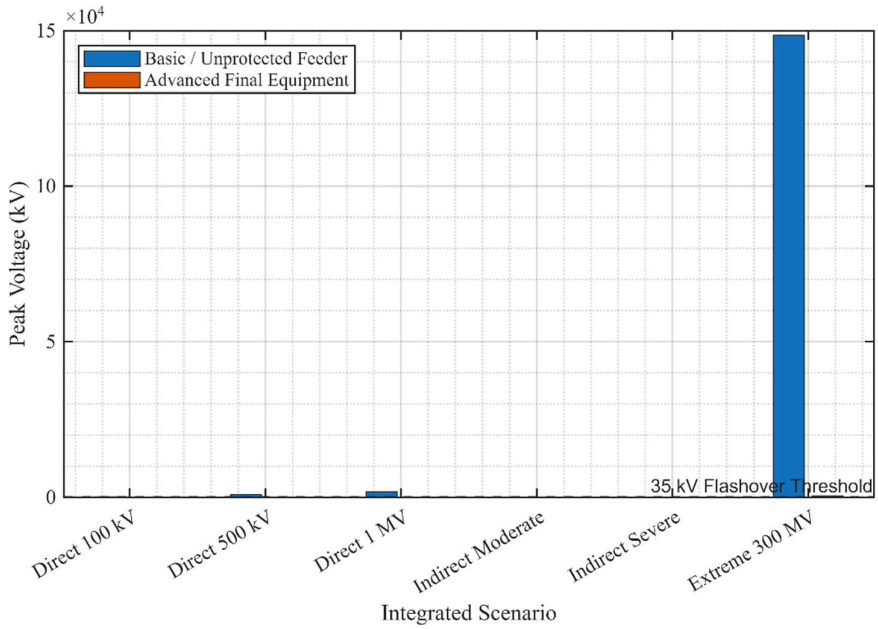

Figure 15. Basic/unprotected versus advanced protected model comparison.

The figure compares unprotected feeder peak voltage, with the final equipment voltage after transformer, MOV and grounding effects, showing overall protection effectiveness.

Table 15 results indicate that at the 100 kV direct surge, the voltage of the feeder (177.33 kV) is decreased to 6.893 kV (96.11% decrease). For the 500 kV case, the voltage decreases from 886.67 kV to 28.28 kV (96.81%). At 1 MV the voltage decreases to 43.81 kV (97.53%), but flashover occurs as a result of exceeding the threshold.

In the case of indirect lightning, the decrease is still high. The moderate case reduces to 1.919 kV, and then to 0.081 kV, with no flashover. The severe case reduces to 47.98 kV, and then to 2.031 kV, and no flashover. The highest reduction (99.69%), however, occurs in the 300 MV extreme case, but the final voltage (454.00 kV) remains above insulation limits

Table 15. Basic/unprotected versus advanced protected model comparison.

Scenario	Source peak (kV)	Basic unprotected feeder (kV)	Transformer sec. A (kV)	MOV-protected A (kV)	Ground rise (kV)	Advanced final equipment A (kV)	Flashover status	Reduction vs basic (%)
Direct 100 kV	100.00	177.33	6.893	6.893	0	6.893	0	96.11
Direct 500 kV	500.00	886.67	34.46	22.20	24.49	28.28	0	96.81
Direct 1 MV	1000.00	1773.33	68.93	22.34	43.81	43.81	1	97.53
Indirect Moderate	3.875	1.919	0.081	0.081	0	0.081	0	95.77
Indirect Severe	96.87	47.98	2.031	2.031	0	2.031	0	95.77
Extreme 300 MV	299995	148586	6290.53	34.00	420.00	454.00	1	99.69

The advanced model, in general, offers a more realistic system-level analysis, including transformer attenuation, MOV clamping, grounding effects, and flashover detection. Although large percentages of voltage reductions are obtained, the findings indicate that insulation safety depends on the final equipment voltage and not on the percentage of voltage reduction.

6. Discussion

The findings show that the proposed integrated lightning protection model offers a more detailed account of the distribution feeder surge behavior as compared to a basic unprotected feeder model. A response of the matrix-coupled three-phase feeder to a surge applied to Phase A only demonstrated that the response can be measured in Phases B and C as well. This confirms that when assessing the lightning induced overvoltage in three phase feeders phase coupling must be taken into account since the adjacent phases may experience lower, but still significant, transient stress [1], [3].

The transformer results indicated that the surge that is transferred to the secondary side is greatly diminished as

compared to the feeder-side voltage. Nevertheless, the transformer is not able to completely remove the transient, which explains the necessity of downstream protection. It was also found that the transformer dynamics can slightly distort the secondary-side waveform making enhanced modeling more appropriate in integrated surge studies [6], [10].

The results of the MOV arrester confirmed effective voltage clamping, and the unprotected output decreased 37.00% to 22.34 kV, confirming that the voltage clamping was effective. Nonetheless, the MOV current was up to 40 kA, and the energy indicator was up to 1398.01 J, which indicated that the performance of the arrester must be evaluated based on the voltage-limiting capability and current-energy stress. This is in line with the simulation studies on surge arrester where the effectiveness of the arrester is determined by both the voltage suppression and discharge stress [15].

Among the most significant study findings was the grounding results. Even though the MOV arrester decreased the local protected voltage, grounding branch brought about ground voltage rise that increased the final equipment voltage. The final equipment voltage was 29.28 kV, which increased to 404.95 kV when the grounding resistance was increased by increasing the grounding resistance of the grounding system and the grounding system itself. This implies that grounding paths and soil dissipation can predominate the final insulation stress, and may offset the advantage of MOV protection, which is also consistent with studies highlighting the importance of grounding paths and soil dissipation to lightning transient behavior [11], [18].

The results of the indirect lightning results indicated that the weak and moderate coupling conditions would result in low final equipment voltages, whereas strong coupling would activate the MOV arrester and cause a high ground voltage rise. The flashover analysis established that insulation safety is dependent on the final equipment voltage as opposed to the insulated voltage with MOVs. In the severe case in the test, flashover was experienced at 25 kV and 35 kV but not at 50 kV or above [12], [20].

The obtained integrated direct surge and scenario comparison results further indicated the significance of considering the entire protection chain. The sophisticated model decreased the equipment level voltage by about 95.77% to 99.69% with respect to the basic feeder response. However, it was still possible to obtain flashover in the 1 MV direct surge demonstration and 300 MV induced demonstration due to the fact that the final equipment voltage was higher than the insulation threshold. Hence, the percentage voltage reduction is not enough; the final equipment voltage, the rise of grounding and flashover margin should be considered jointly.

On the whole, the proposed framework offers a systematic approach to the study of the lightning surge propagation, protection behaviour and insulation risk in distribution feeder systems.

7. Conclusion

The paper has come up with a combined MATLAB/Simulink based lightning protection model to analyze the direct and indirect lightning-induced overvoltage in three phase distribution feeder. The model integrated phase coupling between matrices, RLC feeder response, transformer surge transfer, nonlinear MOV arrester behavior, grounding impedance and flashover detection in a single simulation model.

The findings indicated that the matrix-coupled feeder model was able to model unequal distribution of surges between phases. The transformer minimized the voltage that was transferred to the secondary side and the MOV arrester offered effective clamping of the voltage. Nevertheless, the results of the MOV current and energy were that the arrester stress is still high when there is severe surge events. The grounding analysis revealed that grounding resistance is a significant factor in the final equipment voltage with high grounding resistance leading to large ground voltage rise and high flashover risk.

The integrated model also revealed that the indirect lightning effects are highly dependent on the coupling strength whereas the flashover occurrence is highly dependent on the final equipment voltage relative to the insulation threshold. In the basic-versus-advanced comparison, the advanced protection model decreased equipment-level voltage by an average of 95.77 percent to 99.69 percent. Nevertheless, it was still possible to achieve flashover with extreme cases, which confirmed that the effectiveness of protection should be evaluated based on the final equipment voltage and insulation margin rather than on the basis of the voltage reduction only.

In general, the proposed model offers a useful simulation framework to study the lightning overvoltage propagation and coordination of protection in distribution feeders. Future directions could involve validation of the use of field measurements, detailed manufacturer curves of the arrester, frequency dependent transformer models, soil dependent grounding models and larger configuration of the distribution network.

REFERENCES

1. J. Cao, J. Wang, C. Xu, L. Cai, M. Zhou, W. Chu, *et al*., “Observed induced overvoltage on the test overhead distribution line initiated by natural lightning activities,” *IEEE Transactions on Industry Applications*, 2025.
I. Hetita, D. E. A. Mansour, Y. Han, P. Yang, and A. S. Zalhaf, “Experimental and numerical analysis of transient overvoltages of PV systems when struck by lightning,” *IEEE Transactions on Instrumentation and Measurement*, vol. 71, pp. 1–11, 2022.
2. L. Cai, C. Xu, J. Cao, W. Chu, J. Wang, M. Zhou, and Y. Fan, “Distribution characteristics of induced overvoltage along 10 kV distribution line caused by artificially triggered lightning at 40 m,” *IEEE Transactions on Electromagnetic Compatibility*, vol. 66, no. 1, pp. 195–203, 2023.

I. Hetita, D. E. A. Mansour, Y. Han, P. Yang, C. Wang, and A. S. Zalhaf, "Investigation of induced overvoltages on DC cables of PV system subjected to lightning strikes using FDTD method," *IEEE Transactions on Electromagnetic Compatibility*, vol. 65, no. 4, pp. 1124–1132, 2023.

3. J. Kaushal and P. Basak, "Impact of lightning impulse on the performance of microgrid and low-voltage AC distribution network," in *Proc. 2024 IEEE 13th International Conference on Communication Systems and Network Technologies (CSNT)*, Apr. 2024, pp. 1299–1304.
4. W. Zhao, M. Zhou, Y. Fan, J. Wang, L. Cai, J. Cao, *et al*., "Lightning coupling induced voltage of secondary cables in substation with different terminal load and grounding dissipation paths," *IEEE Transactions on Industry Applications*, 2025.
5. R. A. Moura, A. La Fata, D. Mestriner, A. T. Lobato, and R. Procopio, "Efficient assessment of lightning outages in transmission lines using surrogate models," *IEEE Transactions on Electromagnetic Compatibility*, 2026.
6. S. D. Barman, S. Hossain, R. Shah, S. Islam, S. M. Muyeen, and A. Kumar, "Modeling and analysis of PyroCb lightning leader impacts on PV systems," *IEEE Journal of Photovoltaics*, 2025.
7. H. Huo, D. Wang, H. Chen, C. Zhao, and Q. Cheng, "Considering the methods of lightning protection and early warning for power transmission lines based on lightning data analysis," *IEEE Access*, vol. 12, pp. 54168–54181, 2024.
8. B. Zhang, C. Li, Z. Liu, and J. He, "Analysis of transient in secondary cable due to a direct lightning strike on grounding grid," *IEEE Transactions on Electromagnetic Compatibility*, vol. 65, no. 4, pp. 1183–1190, 2023.
9. M. Zhou, M. Geng, J. Wang, L. Cai, X. Lei, W. Zhao, *et al*., "Lightning-induced transients in buried power cables: A study of soil dissipation effects," *IEEE Transactions on Electromagnetic Compatibility*, 2025.
10. D. Q. Vu, N. N. Nguyen, T. M. T. Le, and P. T. Vu, "Computing lightning-induced voltages on overhead distribution lines using the RBF-FDTD approach," *IEEE Access*, 2025.
11. H. Zhong, J. Chen, Q. Fu, and M. Hua, "Lightning strike identification algorithm of an all-parallel auto-transformer traction power supply system based on morphological fractal theory," *IEEE Transactions on Power Delivery*, vol. 38, no. 3, pp. 2119–2132, 2022.
12. Y. Wang, L. Lei, W. X. Hu, and X. Y. Xiao, "A generic severity estimation method for lightning-caused voltage sags by using multiplatform monitoring data mining," *IEEE Transactions on Power Delivery*, vol. 39, no. 4, pp. 2356–2367, 2024.
13. B. S. Ibrahim, D. M. Soomro, S. Sundarajoo, and M. N. A. Tahrir, "Lightning and surge arrester simulation in power distribution system," in *Proc. 2023 IEEE 8th International Conference on Engineering Technologies and Applied Sciences (ICETAS)*, Oct. 2023, pp. 1–4.
14. C. Hu, S. Lei, Y. Li, and F. Y. Hou, "Decision-dependent resilience enhancement strategy for distribution systems against endogenous wildfires," *IEEE Transactions on Smart Grid*, 2026.
15. M. N. Semenova, Y. V. Bebikhov, and I. A. Yakushev, "Study of normal and emergency modes of operation of the power supply system of industrial enterprises using computer modeling," in *Proc. 2026 International Russian Smart Industry Conference (SmartIndustryCon)*, Mar. 2026, pp. 367–373.
16. F. Grange, S. Journet, H. Rebhi, and F. P. Dawalibi, "Effects of stratified soil structures on indirect lightning-induced overvoltages in HV and MV overhead lines," in *Proc. 2025 International Symposium on Lightning Protection (XVIII SIPDA)*, Sep. 2025, pp. 1–4.
17. J. W. Tang, C. L. Wooi, W. S. Tan, H. N. Afrouzi, S. N. bin Md Arshad, and Y. Von Thien, "Optimization of distribution system reliability using dandelion optimizer," in *Proc. 2023 Innovations in Power and Advanced Computing Technologies (i-PACT)*, Dec. 2023, pp. 1–8.

A. M. Sanchez, X. Yuan, and W. Alvarez, "Comprehensive analysis of lightning-induced faults and SOTF protection malfunctions in 220 kV transmission lines: Case study of Chaglla Hydroelectric Plant," in *Proc. 2025 25th Conference of the Electric Power Supply Industry (CEPSI)*, Oct. 2025, pp. 233–238.

18. H. Qiu, C. Yuting, D. Yajing, H. Tao, S. Congmin, and G. Zhe, "Study on improvement measures for lightning stroke breaking of 10kV overhead insulated conductor in distribution network," in *Proc. 2022 4th International Conference on Electrical Engineering and Control Technologies (CEECT)*, Dec. 2022, pp. 1–5.